Surface Science 662 (2017) 113–122

Contents lists available at ScienceDirect

Surface Science

journal homepage: www.elsevier.com/locate/susc

Stages of Se adsorption on Au(111): A combined XPS, LEED, TOF-DRS, and DFT study

G. Ruano[a,b,1], E. Tosi[a,b,2], E. Sanchez[a,b], P. Abufager[c], M.L. Martiarena[a], O. Grizzi[a,b], G. Zampieri[a,b,*]

[a] Centro Atómico Bariloche (CNEA) and CONICET, Av. Bustillo 9500, 8400 S.C. de Bariloche, Argentina
[b] Instituto Balseiro, UNCU, S.C. de Bariloche, Argentina
[c] Instituto de Física de Rosario, UNR – CONICET, Rosario, Argentina

A B S T R A C T

We have studied the adsorption of Se on the surface Au(111) using XPS, TOF-DRS, LEED and DFT calculations. The use of a doser that operates in vacuum allowed us to investigate all the stages of the adsorption from the clean surface up to the formation of multilayers. In the monolayer regime we have found two ordered phases with distinctive LEED patterns. The LEED pattern of the first phase presents three fractional spots arranged symmetrically around the positions of the spots in a √3x√3 pattern. The analysis of this pattern suggests the formation of either a *nxn* superstructure of √3x√3 domains with n=19 or n=22, or that the adsorption occurs without removing the 22x√3 herringbone reconstruction of the gold surface. This last possibility is in accordance with DFT calculations which show that the charge transfer to a Se adsorbate might not be enough to destabilize the surface reconstruction. Increasing the coverage, beyond 0.3 ML a new LEED pattern appears with broad spots which upon annealing at 150 °C become well defined indicating a 1×8 periodicity. At the highest doses we have observed the formation of multilayers with no discernible LEED pattern. The comparison with adsorption experiments carried out in liquid solutions show similarities and also some important differences.

1. Introduction

There have been a number of studies in recent years of the interaction of sulfur with coinage metals [1–26]. These investigations have been motivated by several reasons, but mainly by the importance of the poisoning effects of sulfur in catalysis and also by the widespread use of thiols (R-SH) and disulfides (RS-SR) to prepare self-assembled monolayers, in which the molecules bind to the surface through the S atom. Although self-assembled monolayers of molecules with heavier chalcogenides (Se and Te) are also of interest because they can provide better electronic conductance and/or stronger bond to the surface, corresponding studies of the interaction of Se and Te with these surfaces are more scarce [27–32]. This motivated us to carry out an investigation of the adsorption of Se on Au(111). Our study was focused on identifying the ordered phases that occur as a function of the surface coverage, and to compare them with those found in the adsorption of S on the same surface [1–14].

In the previous studies of the adsorption of Se on Au(111) the adlayers have been prepared by either immersion in a solution [27,30] or evaporation in vacuum conditions [28]. Lister and Stickney [27] used scanning tunneling microscopy (STM) and low-energy electron diffraction (LEED) to characterize layers grown in an electrochemical cell. Precise control of the potential in the cell allowed them to observe a well-ordered √3x√3 phase at θ = 1/3, and another phase at higher coverage composed of Se octomers (square-like units made of eight Se atoms). All this in good correspondence with results reported for S/Au(111) prepared in similar conditions [1,2,4]. Esaulov et al. [30] used high-resolution x-ray photoelectron spectroscopy (XPS) to characterize layers prepared by immersion in aqueous solutions of $NaSe_2$. The photoemission spectra presented two dominant structures which were assigned in accordance to ref. [27] to Se chemisorbed atomically and to Se octomers; other minor features in the spectra were attributed to other types of polymeric Se conformations. The only previous study with sequential dosing in vacuum conditions was performed by Nagashima [28]. In this study Se was evaporated from a hot tungsten filament and the surface modifications were monitored with Auger

* Corresponding author.
E-mail address: zamp@cab.cnea.gov.ar (G. Zampieri).
[1] Present Address: Instituto de Física del Litoral, UNL – CONICET, Güemes 3450, Santa Fe, Argentina.
[2] Present Address: Nanoproject, Laboratorio de Física del Sólido, Dep. de Física, FACET-CONICET, UNT, Avda. Independencia 1800, S. M. de Tucumán, Argentina.

http://dx.doi.org/10.1016/j.susc.2017.03.009
Received 18 October 2016; Received in revised form 27 February 2017; Accepted 7 March 2017
Available online 13 April 2017

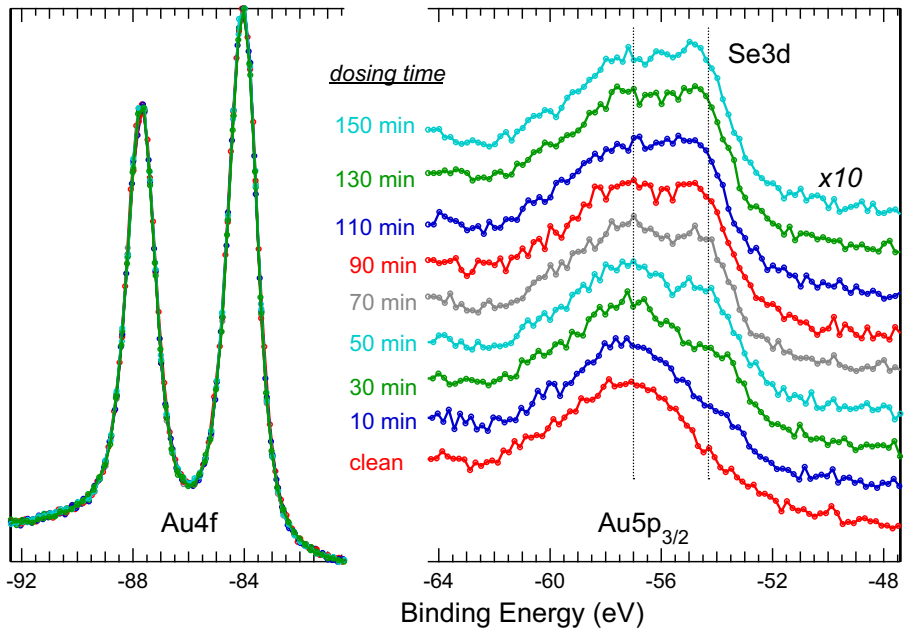

Fig. 1. Photoemission spectra in the regions of the Au4f (left) and the $Au5p_{3/2}$ – Se3d peaks (right) collected as a function of the dosing time. The two vertical lines in the right panel indicate the approximate positions of the $Au5p_{3/2}$ and Se3d contributions. The spectra are presented normalized so that all the Au4f peaks (left panel) have the same intensity.

electron spectroscopy and LEED. From the decay of the Au-69 eV Auger peak the author determined that the growth was layer-by-layer up to the third layer. It is reported that a (√3x√3)R30° LEED pattern was observed with the first monolayer and a weak (1x√7)R79.1° pattern with the second and third layers. In our work both the preparation and the characterization were performed in the same chamber in ultra-high vacuum conditions. The adlayers were grown exposing the Au(111) surface to a beam of Se_2 molecules produced by a solid-state electrochemical cell, and the surface characterization was performed with XPS, LEED and time-of-flight direct-recoil spectroscopy (TOF-DRS). This setup allowed us to explore all the stages of the layer growth, from the submonolayer regime up to the formation of multilayers. At low coverages the LEED pattern shows three fractional spots disposed symmetrically around the positions of √3 spots. At higher coverage, θ ≈ 0.5–0.6, another LEED pattern is observed whose symmetry is not compatible with the formation of Se-octomers as reported in the case of adlayers prepared in liquid solutions. Therefore, similar to the case of S adsorbed on Au(111), it is found that the preparations in liquid and gas phase lead to different high-coverage adlayers.

2. Experimental details

The experimental results reported in this paper were obtained in two different chambers. XPS experiments were performed in a Vacuum Generators chamber equipped with a twin-anode Mg/Al X-ray gun and a hemispherical electrostatic spectrometer, and TOF-DRS experiments were performed in a home-made chamber using a low-energy pulsed Ar^+ beam combined with time-of-flight analysis of the scattered projectiles and recoil target atoms. In this last chamber LEED patterns were also acquired using a rear-view system fitted with a microchannel plate. The base pressure in both chambers was in the 10^{-10} Torr range.

The Au(111) crystal (from Mateck) was prepared by the usual cycles of sputtering an annealing. In the XPS chamber the cycles were continued until the surface was totally free of contaminants, and in the TOF-DRS chamber they were continued until the surface was free of contaminants and the characteristic herringbone LEED pattern was observed.

Se was dosed on the surface by exposing the crystal to a flux generated by a solid-state Ag/AgI/Ag_2Se electrochemical cell. This device was totally similar to that used previously to dose S [3,8,12], with the only change of the Ag_2S pellet being replaced by a Ag_2Se pellet. At typical operating conditions (T ≈ 200 °C and V ≈ 180 mV) the rate of Se deposition was in the order of 1 monolayer/hour. In the XPS experiments the dosage was made in a separate chamber at a base pressure of 10^{-7} Torr, and the sample was then rapidly transferred (in vacuum) to the main chamber for the measurements. In the TOF-DRS experiments the dosage was made *in situ*.

The photoemission spectra were acquired with Al K_α photons (hν = 1486.6 eV). After each Se deposition we measured survey spectra to check the surface cleanliness, and then narrow spectra of selected core-level peaks; these latter were acquired with a pass energy of 20 eV, yielding a total resolution of 1.1 eV as estimated from the width of the $Au4f_{7/2}$ core-level peak. The binding energy (BE) scale was calibrated with the position of the $Au4f_{7/2}$ peak set at 84 eV.

The time-of-flight analysis of the projectiles and recoil atoms was performed by using a detector (channel electron multiplier) placed at the end of a drift tube (L = 176 cm) set at 45° with respect to the incidence beam direction. At the energies of the scattered and recoil particles (keV range) both neutral and charged species are detected with similar sensitivities, thus avoiding uncertainties due to electron exchange processes.

3. Results

3.1. Photoemission spectroscopy

Fig. 1 shows a series of photoemission spectra collected as a function of the dosing time. The spectra are normalized so that all the $Au4f_{7/2}$ peaks have the same intensity (left panel). The most intense peak of Se (3d) falls in the same region as the $Au5p_{3/2}$ peak, thus the Se adsorption is evidenced by the growth of a new feature on the low-BE side of the $Au5p_{3/2}$ peak (right panel).

A close inspection of the shoulder due to the Se3d suggests that the center of gravity of this contribution shifts to larger BE's with the dosing time. This observation is confirmed by a fitting of the spectra with two components, one for the $Au5p_{3/2}$ peak and another for the Se3d contribution, which yields a shift of the Se3d position of about 0.9 eV. In view of this result we performed a new fitting with three components, one for the $Au5p_{3/2}$ peak and two for the Se3d contribu-

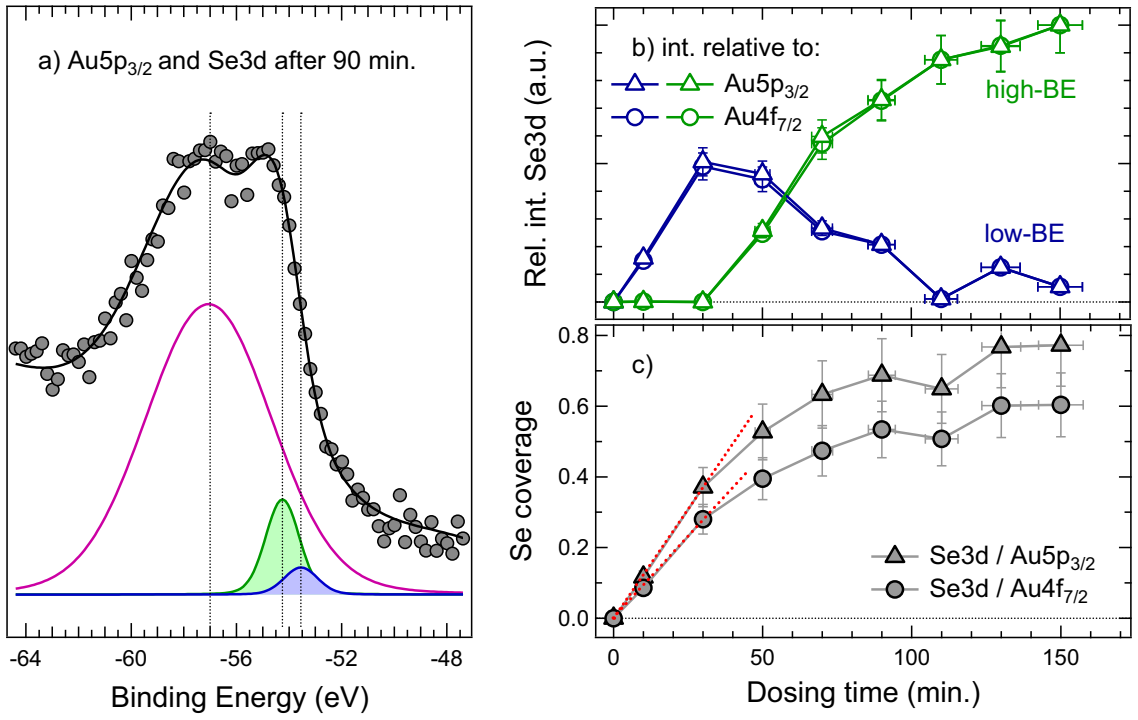

Fig. 2. (a) Photoemission spectrum in the $Au5p_{3/2}$ – Se3d region acquired after 90 min dosing time; the black line on the spectrum is the best fit with three components; the components shown in the lower part correspond to the two Se3d subcomponents (blue and green) and the $Au5p_{3/2}$ peak (violet). (b) Intensities of the Se3d subcomponents, relative to the intensities of the $Au5p_{3/2}$ (triangles) and $Au4f_{7/2}$ (circles) peaks, plotted as a function of the dosing time (note: the intensities relative to the $Au4f_{7/2}$ peaks are presented multiplied by 12.7). (c) Se coverages derived from the ratios of the total Se3d contribution to the $Au5p_{3/2}$ (triangles) and $Au4f_{7/2}$ (circles) peaks, plotted as a function of the dosing time. (For interpretation of the references to color in this figure legend, the reader is referred to the web version of this article.)

tion. The $Au5p_{3/2}$ peak was represented by a single Voigt function; the position and width of this component were determined with the spectrum of the clean sample and kept fixed thereafter. The Se3d contribution was accounted for with two spin-orbit split doublets, each one represented by a pair of Voigt functions with fixed intensity ratio (3:2) and fixed separation (0.86 eV). To keep the number of fitting parameters to a minimum the widths of these Voigt functions were kept fixed at 1.4 eV and the positions of the $3d_{5/2}$ peaks were fixed at the values found in refs. [30] and [33]: 53.55 and 54.25 eV. All the spectra could be fitted satisfactorily varying only the intensities of these three components and a Shirley-type background [34].

Fig. 2(a) presents the result of the fitting in the case of the spectrum acquired at t = 90 min. Although the Se3d photoemission cross-section is approximately a factor of two larger than that of the $Au5p_{3/2}$ core level [35], the Au peak is considerably bigger because of the larger number of layers contributing to it [36].

The intensities of the two Se3d doublets are presented in Fig. 2(b) plotted against the dosing time. The intensities are shown referred to the intensity of the $Au5p_{3/2}$ peak (triangles) obtained in the same fitting and to the intensity of the $Au4f_{7/2}$ peak (circles) obtained in another fitting [38]. It can be seen in this figure that the evolutions of the Se3d subcomponents are practically the same, irrespective of which Au peak they are referred to. The most important finding, however, is that during the first part of the adsorption only the low-BE component is present. The intensity of the high-BE component is almost zero during the first 30 min and then starts to increase becoming rapidly the main component. The low-BE component reaches its maximum at 30 min and then decreases continuously.

The Se coverage can be determined from the intensity ratio between the Se3d peak and any of the two Au peaks; to this purpose the intensities must be divided by the corresponding photoemission cross sections and the Au signals must be divided also by the mean number of Au planes contributing to the peak (as given by the respective attenuation lengths divided by the (111) interplane separation). Therefore, the intensity ratios between the Se3d peak and the $5p_{3/2}$ and $4f_{7/2}$ Au peaks provide two independent determinations of the coverage, and both results are presented in Fig. 2(c). It is seen that the two curves exhibit the same behavior, although there is a small difference between them. This difference must be ascribed to errors in the values used for the cross sections of the Au peaks and/or the attenuation lengths of the corresponding photoelectrons; however, since these latter depend only on the kinetic energies which in the case of the 4f and 5p core levels differ in only 2%, we think that the difference is more likely due to errors in the photoemission cross sections. Leaving aside this small discrepancy in the absolute value of the coverage, it can be seen in both cases that the Se coverage increases linearly during the first 30 min, after which it continues increasing but at a smaller rate. Interestingly, the region of linear increase coincides with the existence of only the low-BE component in the spectrum, and the limit of this region occurs when the coverage has reached a value close to 1/3 monolayer (ML), which is the coverage of a $\sqrt{3}x\sqrt{3}$ arrangement of atoms. With these observations it seems natural to ascribe the low-BE component to Se atoms chemisorbed in hollow sites, with a $\sqrt{3}x\sqrt{3}$ type of long-range ordering, as made in ref. [30]. With regards to the high-BE component, it must correspond to Se atoms in other environments, conforming a phase of higher coverage. Although it is tempting to ascribe this component to Se octomers as observed in ref. [27], it will be shown below that these units might not be formed in our experiment.

3.2. Ion-scattering and recoil spectroscopy

Fig. 3 presents a typical TOF-DRS spectrum acquired at an intermediate stage of the adsorption process. The main features in the spectra are: i) an intense narrow peak at 12.8 μs corresponding to Ar projectiles scattered off Au substrate atoms, ii) a structure on the right flank of the previous peak (here appearing as a shoulder) that corresponds to Ar projectiles scattered off Se atoms, iii) a smaller

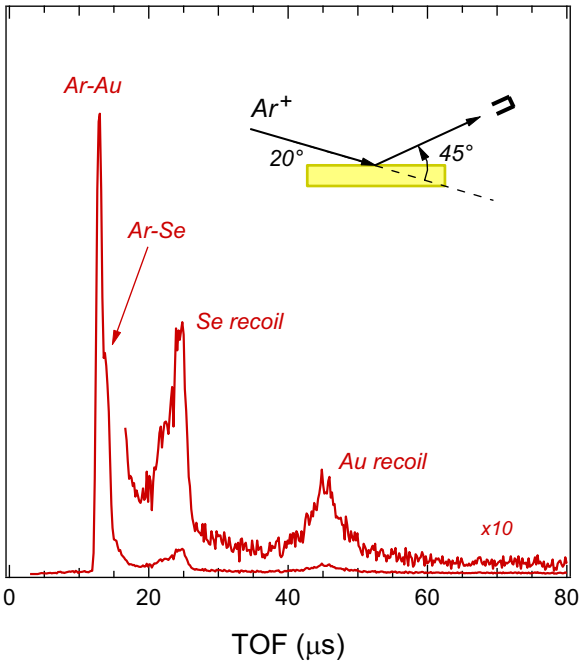

Fig. 3. Typical TOF-DRS spectrum measured at an intermediate stage of the Se adsorption process. The two scattering peaks and the two recoil peaks are indicated The inset shows the geometry of the acquisition; the incidence and scattering angles are 20° and 45°, respectively; the plane of scattering is along the [112] azimuth.

structure at around 25 μS due to Se atoms ejected from the surface in quasi-single collisions, and iv) a similar structure at around 45 μs corresponding to Au atoms ejected from the surface. The first two structures will be referred to generally as Ar scattering peaks, labelled Ar-Au and Ar-Se in the graph, and the last two as recoil peaks. Light adsorbates such as H or C should appear at the left side of the Ar-Au peak; their absence in the spectrum of Fig. 3 implies a very clean surface.

The low acquisition times and low irradiation damage characteristic of TOF-DRS allow to monitor the adsorption process continuously, maintaining thereby the doser in a steady condition. Fig. 4 shows a series of spectra collected while the surface was being exposed to the Se flux. Note that these experiments were performed in a different chamber, and so the dosing times do not necessarily match those used in the photoemission experiments. Panel (a) shows the region of the two scattering peaks, and panels (b) and (c) the regions of the two recoil peaks. The last two spectra in each panel, labeled “infinite”, were recorded after exposing the sample a long time to the doser operating in a high-flux condition; they are presented superimposed to stress that they are completely similar, implying that the surface region contributing to the spectra has reached a steady state and does not change anymore.

It is seen in Fig. 4 that the increase of the two Se peaks is accompanied by a decrease of the two Au peaks. Panel (a) shows that the Ar-Au peak dominates in all the spectra of the series up to the longest time (350 min), and that its TOF position remains almost unchanged; this indicates that there are Au atoms in the top layer free for scattering and that the Se coverage is still in the monolayer regime. In the last two spectra (labelled “inifinite”), acquired after heavy Se dosing, the Ar-Au peak is totally suppressed and only the Ar-Se peak remains. This situation must correspond, therefore, to the surface covered by a Se multilayer.

A close inspection of the spectra in panels (b) and (c) of Fig. 4 reveals that the evolution of the recoil peaks is not smooth. The Se recoil peak (panel (b)) initially grows as a single narrow peak at 25.5 μs, then becomes broader and shifts toward lower TOF, and additionally, at around 200 min a shoulder develops and grows at the left side of the peak. Interestingly, in the last two spectra, when the surface has been covered with a Se multilayer, the position of the main peak reverts to the position at the beginning of the adsorption. The Au recoil peak (panel (c)) also exhibits a non uniform behavior. Initially the peak decreases more or less continuously until at around 100 min where it seems to stabilize, and later, at around 180 min it decreases again rather rapidly. All these changes evidence variations in either the Se sticking and/or the arrangement of the atoms that give rise to shadowing or blocking effects of the trajectories.

To gain insight into the evolutions of the recoil peaks we fitted them with Gaussian functions. Three Gaussian functions were enough to achieve satisfactory results. Two illustrative examples of the fittings are shown in panels (a) and (b) of Fig. 5. The peak areas and the position of the main peak in the case of the Se recoil are presented plotted against the dosing time in panels (c) to (e); at the far right we have plotted the intensities and positions obtained in the fitting of the two spectra labeled “infinite” in Fig. 4.

In the variation of the Au intensity (panel (c)) one can distinguish several regions: a nearly linear decrease since the beginning of the dosing until around 100 min; a change in the slope reaching a plateau or slight increase between 100 and around 150 min; a new decrease until around 200 min and then another plateau with a small but nonzero intensity. As mentioned above the peak disappears completely only after heavy dosing which leads to the formation of multilayers (spectra labeled “infinite” in Fig. 4).

In the case of the Se recoil there are two components with different behaviors. Initially the spectrum is composed of a single peak whose intensity increases linearly with the dosing time; at around 150 min the intensity of this component decreases slightly and then grows again reaching a region with small variations at around 300 min. The second component located at 3–4 μs smaller TOFs is initially zero until it makes a sudden appearance at around 70 min; after this dosing time it increases continuously, passes a region of small variation between 250 and 350 min, and then increases again reaching a high value in the region of the Se multilayer. Finally, panel (e) shows that the position of the main peak undergoes a small but noticeable change from around 25.5 μs at low dosing times to around 24.8 μs at high dosing times.

The existence of more than one component in the spectra of the recoils reflect the fact that these peaks are formed not only by the true single collision contribution but also by atom trajectories involving some sort of multiple paths resulting from collisions with neighboring atoms. In fact, due to the high density of the Au(111) surface most of the Au recoil contribution comes from the latter. In the case of Se, at the beginning of the adsorption the recoils form a single narrow peak at the TOF of a true single collision, meaning that the Se atoms are spread out and above the Au top layer, i.e., not forming an alloy or immersed in the substrate. The second peak at lower TOF, associated to multiple collisions, appears at around 70 min; since this time coincides with the first observation of a LEED pattern described below, we interpret that the appearance of this peak marks the onset of ordered island formation. The other changes that occur between 150 and 200 min, particularly the decrease of the main peak with increasing dose and its change of position, are ascribed to rearrangements of the surface atoms to form a new phase, characterized by the high-binding energy component of the XPS spectra and a different LEED pattern, as described below.

3.3. Low-Energy Electron Diffraction

Two different LEED patterns were found during the adsorption; they are presented in the panels (a) and (b) of Fig. 6. The horizontal axis at the top of the figure indicates the dosing-time intervals in which each pattern was observed.

The pattern shown in panel (a) resembles that of a (√3x√3)R30° phase, but a close inspection of the fractional spots reveals that they are composed of groups of three spots. This is clearly seen in panel (c),

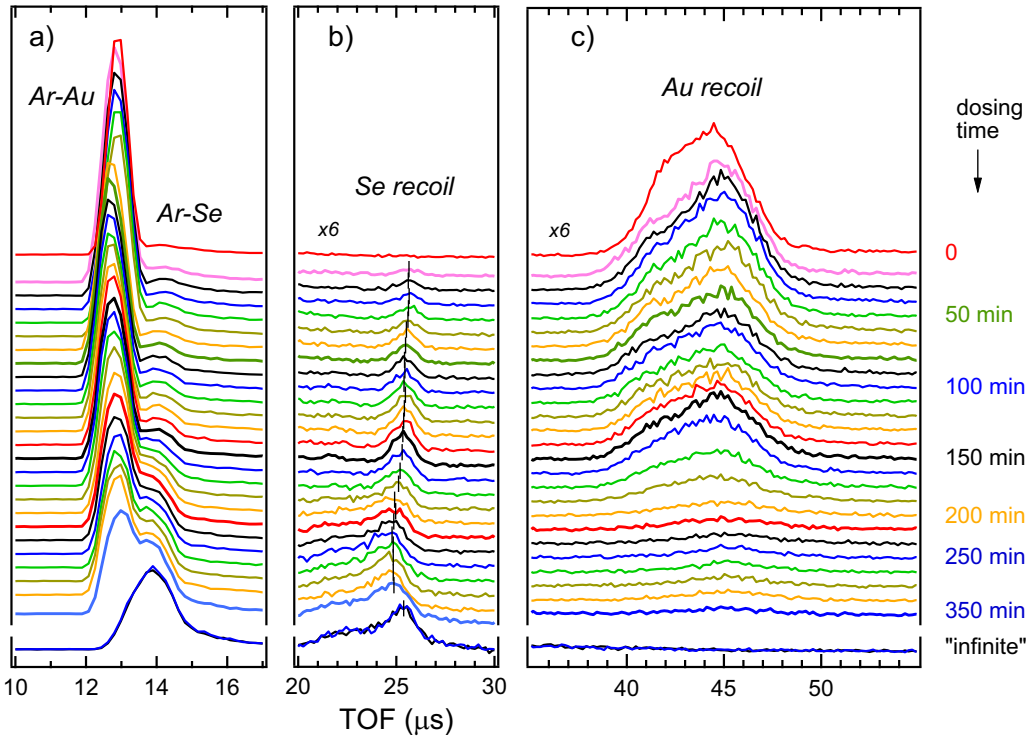

Fig. 4. TOF-DRS spectra acquired while the surface was exposed to the Se flux; the dosing times are indicated on the right. (a) Region of the scattering peaks, (b) region of the Se recoil, and (c) region of the Au recoil. The vertical bars in panel (b) indicate the position of the maximum. (Note: this experiment was performed in a different chamber and so the dosing times do not match those used in Figs. 1 and 2).

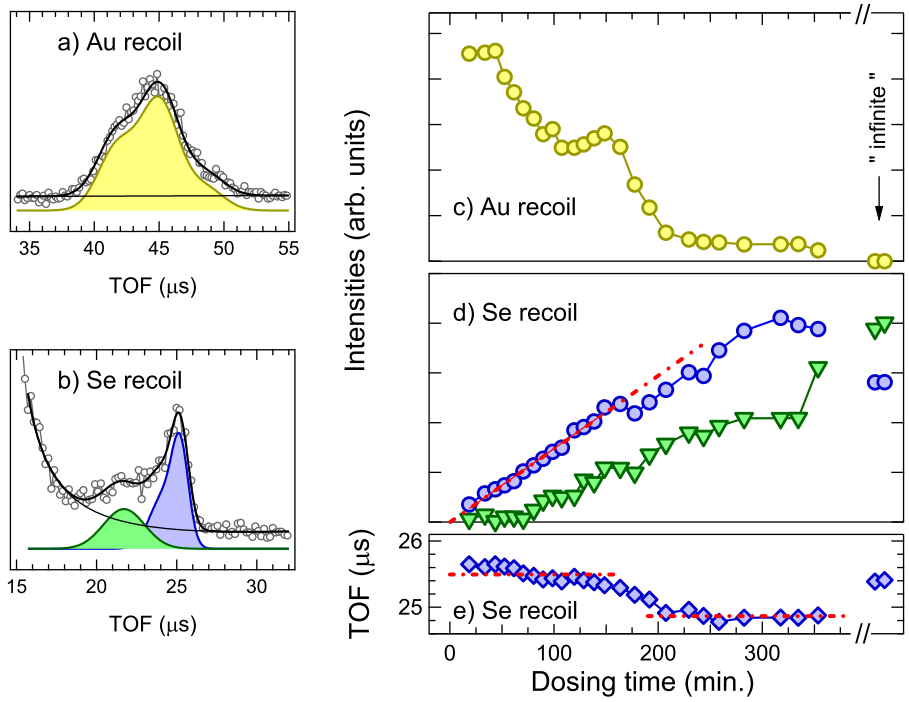

Fig. 5. (a) Fitting of the Au recoil peak at 190 min; (b) same for the Se recoil peak; (c) total area of the Au recoil peak plotted against the dosing time; (d) areas of the main (blue circles) and secondary (green triangles) peaks in the spectrum of the Se recoil; (e) position of the main peak in the spectrum of the Se recoil. (For interpretation of the references to color in this figure legend, the reader is referred to the web version of this article.)

where a pattern acquired at a smaller electron energy is presented; for this reason this pattern will be referred to hereafter as “pseudo-√3”. At dosing times longer than 200 min the pseudo-√3 pattern disappeared and a new pattern, shown in panel (b), emerged and was observed until the longest dosing times. When the sample was annealed at 150 °C the spots became better defined and some more spots became visible, as it is shown in panel (d). On the contrary, when the Se dosing was increased to form multilayer the LEED pattern disappeared completely, but upon annealing at 150 °C the pattern of panel (d) was immediately recovered. The positions of the fractional spots in the pattern of panel (d) suggest a 1×8 periodicity in real space. It must be mentioned, however, that at low energies we have also observed the appearance of

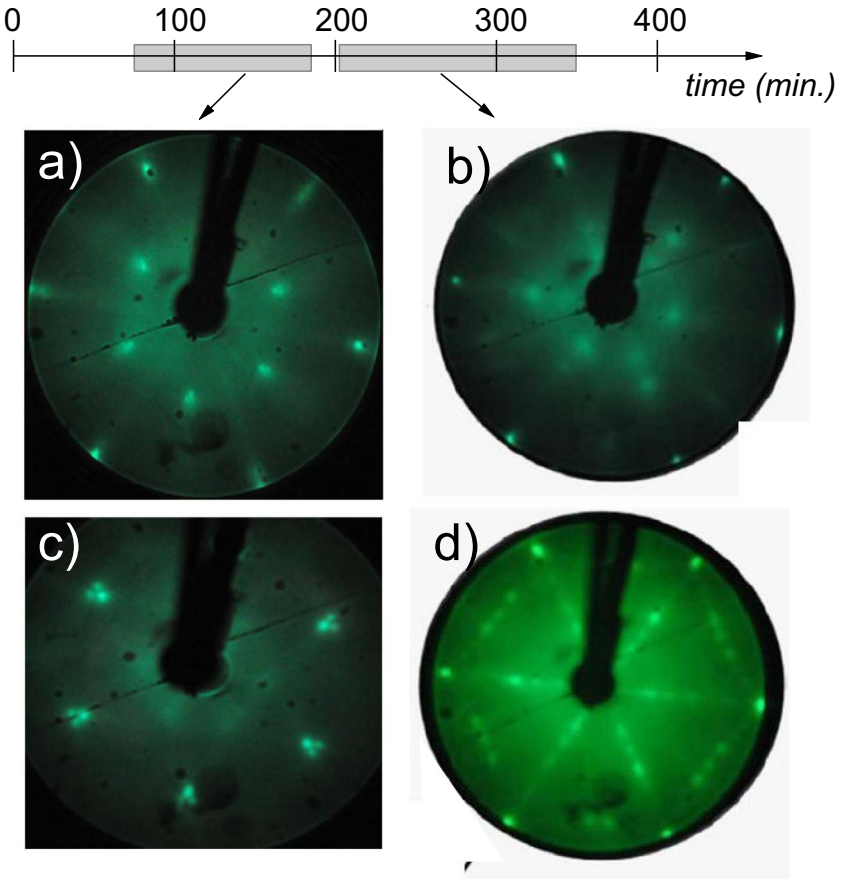

Fig. 6. (a) LEED pattern observed between approximately 70 and 180 min (E = 72 eV); (b) LEED pattern observed above 200 min (E = 68 eV); (c) same pattern of panel (a) but acquired with E= 36 eV; (d) pattern of panel (b) after annealing the sample at 150 °C (E = 69 eV).

blurred spots in intermediate positions.

4. Discussion

To advance in the analysis of the results we need to convert the scale of dosing time in the TOF-DRS/LEED chamber into coverage. To this purpose we note that the initial evolution of the recoil intensities, particularly the linear increase of the main peak of the Se recoil, and the observation of the pseudo-√3 LEED pattern until dosing times about 180 min are in good correspondence with the initial evolution of the XPS data, where the Se3d spectrum exhibits only one component whose intensity grows also linearly with the dosing time. Thence, we postulate that 180 min dosing time in the TOF-DRS/LEED experiment must correspond to a coverage θ ≈ 0.3. Having established this connection between the experiments made in the two chambers we come to an scenario for the Se adsorption similar to that found previously for the S adsorption [5–10,12,13]; namely the existence of two phases with distinctive LEED patterns at coverages smaller and larger than θ ≈ 0.3. One must note, however, that in the case of S adsorption a "true" (√3x√3)R30° phase has also been detected in a limited range around 1/3 ML [8,10,12,13], but this phase has not been observed in the present experiment.

In the following we will analyze the periodicities and atomic structures that are implied by the two LEED patterns. This is made comparing the measured LEED patterns with patterns calculated for different arrangements of Se atoms. The LEED intensities are calculated in the frame of the kinematical model and considering only one layer of Se atoms. It will be shown below that these simple calculations are sufficient to discriminate among different models (see also ref. [8]).

4.1. Low-coverage phase

To begin with the analysis of the phase characterized by the pseudo-√3 pattern, we recall that the low-coverage phase of S/Au(111) is also characterized by a LEED pattern with three fractional spots around the positions of the √3 spots [8,10,12,13]. The analysis of that pattern showed that the fractional spots were part of a (1/5)x(1/5) sublattice, implying a 5×5 periodicity in real space [8]. This is a special case of diffraction from domain-wall systems treated in reference [39]. These systems composed of √3x√3R30° domains ordered in the long-range with *n*x*n* periodicity have characteristic LEED patterns with bright fractional spots located in the vicinity of the √3-spots. As *n* increases the distance between the spots decreases as 1/*n* and the systematic of the bright fractional spots is as follows: when *n* is a multiple of 3 one fractional spot coincides with the √3-spot and it is accompanied by a hexagon of six nearest fractional spots; in all the other cases there is a triangle of three fractional spots centered at the √3 position with one vertex pointing to the origin if *n* is just smaller than a multiple of 3 or away from it if *n* is just greater than a multiple of 3. Therefore, if our pseudo-√3 pattern corresponds to a *n*x*n* superstructure of √3x√3R30° domains *n* must be 19 or 22 (these two cases cannot be distinguished with the present data).

The unit cell derived above in the assumption of a *n*x*n* arrangement of √3 domains is suggestively close to the periodicity of the herringbone reconstruction of the clean gold surface. Therefore, we have also considered the possibility that the 22x√3 reconstruction of the clean surface may persist during the Se adsorption. To find out if this scenario is compatible with the pseudo-√3 pattern we simulated LEED patterns assuming different configurations of Se atoms adsorbed on the reconstructed surface. One of these configurations is shown in the top panel of Fig. 7.

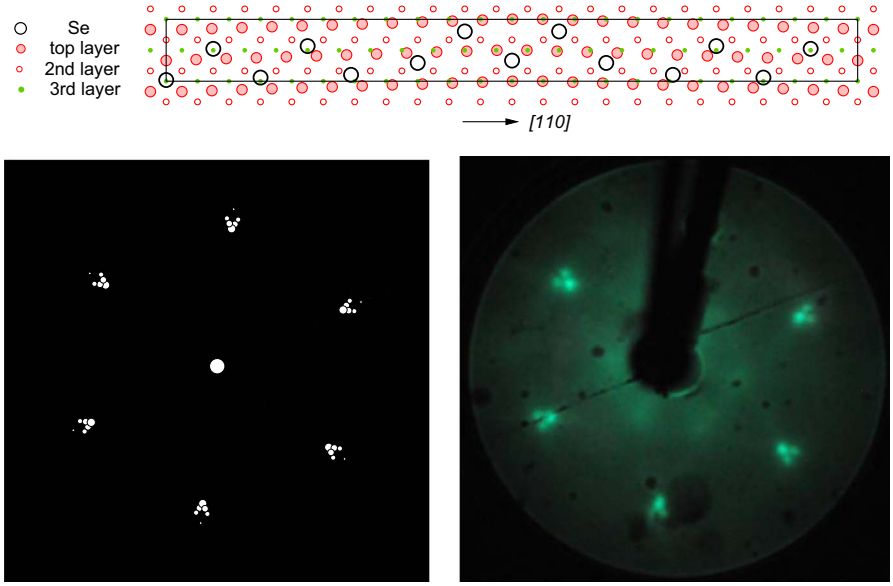

Fig. 7. Comparison of the LEED pattern calculated for the configuration of 14 Se atoms shown in the top panel (on the 22x√3 unit cell of the herringbone reconstruction) with the LEED pattern presented in Fig. 6(c).

As it is known in the herringbone reconstruction the interatomic distance along one [110] direction is contracted by 4% to host a new Au atom every 22 atoms [40,41]. We have considered configurations of Se atoms adsorbed on this reconstructed surface subject to two conditions: 1) the adsorbates sit on 3-fold hollow sites, and 2) the adsorbates maintain as much as possible a √3x√3 type of coordination. It must be noted that in the reconstructed Au surface there are three types of 3-fold hollow sites: "hcp", above a 2nd layer atom, "fcc", above a third layer atom, and a new type that we will call "empty", above a fourth layer atom; in the top panel of Fig. 7 the "empty" sites appear in the center zone while the "hcp" and "fcc" sites appear in the left and right borders of the unit cell. For each configuration we calculated the intensities of the fractional spots in the frame of the kinematical model and compared the LEED patterns with the measured one. The best result was obtained with the configuration shown in the top panel of Fig. 7, in which the Se atoms occupy "empty" sites at the center of the unit cell and "fcc" sites at the two sides of the unit cell. Since pure √3-coordination cannot be realized in the 22x√3 unit cell, the atomic arrangement has two fault lines at about 1/3 and 2/3 of the unit cell. It can be seen in the bottom part of Fig. 7 that the simulated LEED pattern has bright fractional spots in very good agreement with those of the measured pattern [42]. Additionally, the maximum coverage with this configuration of Se atoms is θ = 0.304 (14/46), which agrees well with the upper limit of the range of coverage in which the Se-3d photoemission peak has only one component whose intensity increases linearly with the dosing.

Therefore, the pseudo-√3 LEED pattern is consistent with both a) a *n*x*n* superstructure of √3x√3R30° domains with *n* = 19 or 22, and b) adsorption on the 22x√3 unit cell of the reconstructed Au(111) surface.

Since both scenarios are quite different from the case of S adsorption, we performed DFT calculations to elucidate the origin of the different behaviors. The calculations considered one S or Se atom in 6×6, 5×5, and 3×3 unit cells of a perfect Au(111) surface, with corresponding coverages θ = 1/36, 1/25, and 1/9 [43]. In all the cases we found that the lowest-energy adsorption sites were fcc sites. Table 1 shows the distances to a substrate atom and the charge transfer to the adsorbates. It is seen that the Se-Au bonds are always longer than the S-Au bonds, what is ascribed to the larger atomic size of Se. But the most interesting finding to understand the different behaviors of S and Se is related to the excess charge around each adsorbate.

It can be seen in Table 1 that the charge transferred to a S adsorbate is 3 to 5 times larger than that transferred to a Se adsorbate. This is important because it is known that removal of electronic charge from the topmost Au layer destabilizes the herringbone reconstruction [47]. In the case of S it has been reported that the lifting of the reconstruction begins to occur at around θ = 0.05 and is almost complete at θ = 0.1 [10]; since these two coverages correspond to around 2 and 4 adsorbates per (22x√3) unit cell, according to Table 1 the lifting of the reconstruction begins to occur with the loss of around 0.5e per (22x√3) unit cell and is complete with the loss of around 1e per unit cell. In the case of Se, however, due to the much smaller charge transfer such electron losses per unit cell would occur at coverages θ ≈ 0.2 and 0.5, what makes plausible the suggestion made above that the herringbone reconstruction may persist during the Se adsorption.

Table 1
DFT results for S and Se adsorbed on a perfect Au(111) surface.

unit cell	θ	S/Au(111)		Se/Au(111)	
		d_{min} [Å]	$\delta n = n_e - 6$	d_{min} [Å]	$\delta n = n_e - 6$
6×6	1/36	2,44	0.27	2.53	0.09
5×5	1/25	2,41	0.24	2.49	0.06
3×3	1/9	2.41	0.20	2.49	0.04

d_{min} is the minimum distance to a Au atom; n_e is the mean number of valence electrons around an adsorbate.

4.2. High-coverage phase

According to refs. [27] and [30] the high-coverage adlayers prepared in liquid solutions contain Se octomers. Lister and Stickney reported STM images of large patches of the surface in which the octomers are ordered as depicted in the left panel of Fig. 8. It is immediately apparent that the periodicity of this superstructure is not consistent neither with the 1×8 periodicity implied by the LEED pattern of our high-coverage phase nor with the (1x√7)R79.1° periodicity reported by Nagashima [28]. Additionally, the coverage of this array of octomers, θ = 8/9, is considerably larger than the coverages at which the 1×8 pattern is observed in our experiment. In spite of these differences we calculated the LEED pattern corresponding to this supercell, which is shown in the right panel of Fig. 8. As expected, the simulated pattern does not compare with our pattern, having many more bright spots. Therefore, we must conclude that the adsorptions in liquid and vapor phase lead to different results.

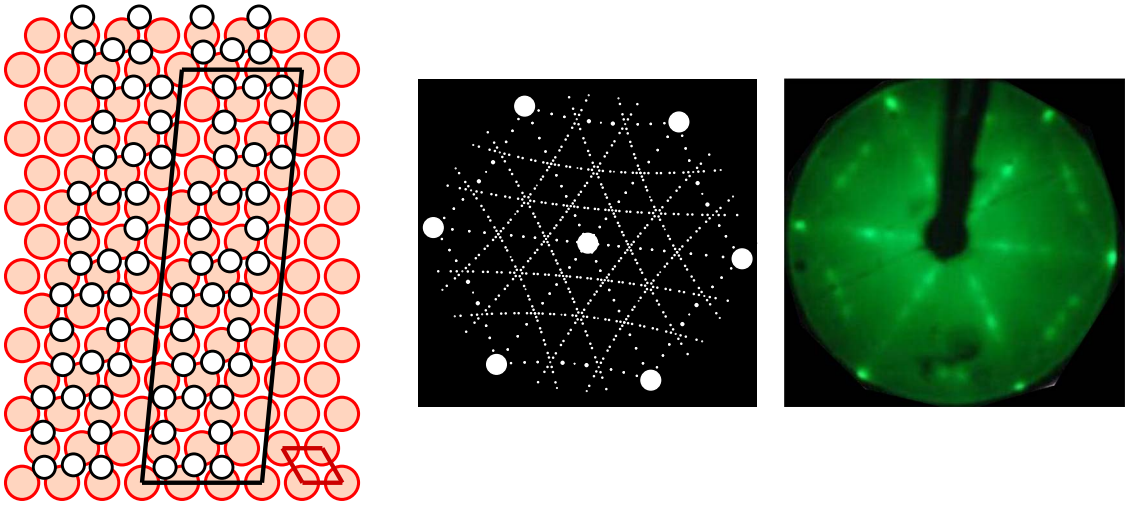

Fig. 8. Left: array of Se-octomers observed in the experiment of reference [27]; the unit cells of the clean surface and the superstructure are shown in red and black, respectively. Right: comparison of the LEED pattern calculated for the model on the left (in the kinematical approximation) with the LEED pattern of the high-coverage phase presented in Fig. 6(c). (For interpretation of the references to color in this figure legend, the reader is referred to the web version of this article.)

The approach used above to analyze the atomic structure of the low-coverage phase does not provide conclusive answers in this case because many configurations of Se atoms yield similar LEED patterns. It is evident, therefore, that a more complex model and/or more sophisticated calculations are needed in this case. In spite of this, a couple of rules emerging from our simple calculations might be significant. Firstly, all the configurations that yield reasonable agreement have between 4 and 6 atoms in the 1×8 unit cell, what is consistent with the range of coverages in which the LEED pattern is observed. Secondly, the configurations with the atoms grouped in pairs give in general better results than the configurations with the atoms more evenly spaced. This prevalence of the configurations with the adsorbates grouped in pairs is in accordance with the finding in the similar S/Au(111) system that when the coverage increases the bonds with the substrate atoms weaken and this favors the formation of bonds among adsorbates [3,4,11]. Having the Se atoms grouped in pairs or small clusters may also be in better agreement with TOF-DRS results where a strong multiple scattering contribution is present for this high coverage phase. If the Se atoms were more spread out or isolated, as happens at the beginning of the adsorption, the Se recoil peak should keep increasing till completion of one full monolayer without the strong changes, shoulders and additional peaks observed, as described above.

4.3. Comparison of the adsorptions in liquid and vapor phase

In principle, one would expect to find the same ordered phases regardless of the environment in which they are prepared. Therefore, it is of interest to compare the reports of S and Se adsorptions carried out in vacuum and electrochemical cells to see to which extent this rule is fulfilled.

4.3.1. Low-coverage phase

We begin with the analysis of the S adsorption. Initially both wet and dry preparations reported the existence of a (√3x√3)R30° ordered phase. While Rodriguez et al. [3] and Biener et al. [6] identified this phase in experiments performed in vacuum by the characteristic LEED pattern, Salvarezza et al. [1,2,4] reported STM images of surface regions with this ordering in experiments carried out in Na_2S solutions. Some time later, however, new reports of experiments performed in vacuum showed that the blurred fractional spots of the LEED pattern were actually three spots disposed symmetrically around the positions of the √3 spots [8,10]. As mentioned above, these new spots imply a 5×5 periodicity in real space, and a new arrangement of atoms was proposed that retains √3 coordination in the short range but not in the long range [8,13]. A proper (√3x√3)R30° phase was observed only in a narrow range around 1/3 ML, and it was seen to be rather unstable [8].

In the case of Se, Lister and Stickney reported the formation of a well ordered (√3x√3)R30° phase in experiments performed in an electrochemical cell with a SeO_2 solution; they observed both a good LEED pattern and STM images of large surface patches covered with atoms in that arrangement [27]. In our experiment conducted in vacuum, however, we observed a LEED pattern with three spots around the positions of the √3 spots, the closeness of which implies the existence of a very large supercell, again with local √3x√3 order of the atoms.

Therefore, while the adsorptions of both S and Se in liquid media led to the formation of a (√3x√3)R30° ordered phase, the adsorptions in vacuum led to slightly different results. Perhaps the reason for these differences is that the two types of experiments emphasize different aspects of the problem. While the experiments performed in vacuum offer the possibility to investigate intermediate coverages, in some cases one may face difficulties to stabilize specific phases (ex.: the (√3x√3)R30° phase of S/Au(111)). On the contrary, in an electrochemical cell some phases of intermediate coverage may be difficult to stabilize and others be clearly favored. Additionally, one should also consider that the potential applied to promote the adsorption may destabilize the reconstruction of the clean surface [48]; if this occurred the adsorptions in vacuum and the cell would take place in different scenarios.

4.3.2. High-coverage phase

The existence of a distinct ordered phase at high coverage has been reported for both types of preparations and for both types of adsorbates.

The landmark of the experiments carried out in liquid solutions is the formation of octomers. These square-like structures composed of 8 atoms have been observed by STM for both S and Se. In both cases the images show also that the octomers are arranged with certain ordering (different for S and Se), but no LEED pattern has been reported.

When the adsorptions are made in vacuum the common feature is that the high-coverage phase becomes well ordered only after a mild surface annealing. In the case of S the first observation of a high-coverage phase was made by Oudar et al., who identified a phase with θ = 0.5 and a well-defined but complex LEED pattern [49]. The subsequent experiments confirmed the LEED pattern [8,10,12,13] and added some STM images [8,10]. Rather surprisingly, however, neither the STM images nor the complex LEED pattern seem consistent with an ordered array of octomers [8]. A similar situation is

encountered in the case of Se. As shown above, the high-coverage phase has a characteristic 1×8 LEED pattern which also seems incompatible with any model based on octomers.

Therefore, while the experiments performed in liquid phase coincide in the formation of octomers, no evidence of such structures is found in the experiments performed in vacuum.

5. Conclusions

The use of a Se doser operated in vacuum allowed us to analyze the different stages of the Se adsorption on Au(111). With a combination of XPS, LEED and TOF-DRS we have identified two ordered phases: one extending up to around $\theta \approx 0.3$, and another one at higher coverages that becomes well defined only after a mild annealing. The LEED pattern of the low-coverage phase implies either a 19×19 or 22×22 supercell with adsorbates in local √3x√3 order or that the adsorption preserves the 22x√3 herringbone reconstruction of the Au(111) surface. We performed DFT calculations finding that the charge transfer from the Au surface atoms to a Se adsorbate is between 3 and 5 times smaller than that to a S adsorbate, what might be the cause of the different behaviors of Se and S. The LEED pattern of the high-coverage phase suggests a (1×8) periodicity, but the most important finding is that the pattern would not be consistent with the array of Se-octomers observed when the adsorption is carried out in an electrochemical cell. This means, therefore, that as in the case of S adsorption, the experiments performed in vacuum and liquid solutions give high-coverage phases of different nature.

Acknowledgments

This work has been supported in part by grants from CONICET (PIPs 112–201101- 00650, 112–201101- 00594), Universidad Nacional de Cuyo (06/C402, 06/C454), and ANPCyT (PICT 01242).

Appendix A. Supporting information

Supplementary data associated with this article can be found in the online version at doi:10.1016/j.susc.2017.03.009.

References

[1] G. Andreasen, C. Vericat, M.E. Vela, R.C. Salvarezza, Dynamics of sulfur adlayer transformations at metal/electrolyte interfaces, J. Chem. Phys. 111 (1999) 9457–9460.
[2] C. Vericat, M.E. Vela, G. Andreasen, R.C. Salvarezza, L. Vázquez, J.A. Martín-Gago, Sulfur–substrate interactions in spontaneously formed sulfur adlayers on Au(111), Langmuir 17 (2001) 4919–4924.
[3] J. Rodriguez, J. Dvorak, T. Jirsak, G. Liu, J. Hrbek, Y. Aray, C. González, Coverage effects and the nature of the metal-sulfur bond in S/Au(111): high-resolution photoemission and density-functional studies, J. Am. Chem. Soc. 125 (2002) 276–285.
[4] C. Vericat, M.E. Vela, G.A. Andreasen, R.C. Salvarezza, F. Borgatti, R. Felici, T. Lee, F. Renner, J. Zegenhagen, J.A. Martín-Gago, Following adsorption kinetics at electrolyte/metal interfaces through crystal truncation scattering: sulfur on Au(111), Phys. Rev. Lett. 90 (2003) (75506–1).
[5] M.M. Biener, J. Biener, C.M. Friend, Revisiting the S-Au (111) interaction: static or dynamic?, Langmuir. 21 (2005) 1668–1671.
[6] B.K. Min, A.R. Alemozafar, M.M. Biener, J. Biener, C.M. Friend, Reaction of Au(111) with sulfur and oxygen: scanning tunneling microscopic study, Top. Catal. 36 (2005) 77–90.
[7] S.Y. Quek, M.M. Biener, J. Biener, J. Bhattacharjee, C.M. Friend, U.V. Waghmare, E. Kaxiras, Rich Coordination chemistry of Au adatoms in gold sulfide monolayer on Au(111), J. Phys. Chem. B. 110 (2006) 15663–15665.
[8] M. Yu, H. Ascolani, G. Zampieri, D.P. Woodruff, C.J. Satterley, R.G. Jones, V.R. Dhanak, The Structure of atomic sulfur phases on Au(111), J. Phys. Chem. C 111 (2007) 10904–10914.
[9] S.Y. Quek, M.M. Biener, J. Biener, J. Bhattacharjee, C.M. Friend, U.V. Waghmare, E. Kaxiras, Structure of incommensurate gold sulfide monolayer on Au(111), J. Chem. Phys. 127 (2007) 104704. http://dx.doi.org/10.1063/1.2770731.
[10] M.M. Biener, J. Biener, C.M. Friend, Sulfur-induced mobilization of Au surface atoms on Au(111) studied by real-time STM, Surf. Sci. 601 (2007) 1659–1667. http://dx.doi.org/10.1016/j.susc.2007.01.041.
[11] P.G. Lustemberg, C. Vericat, G.A. Benitez, M.E. Vela, N. Tognalli, A. Fainstein, M.L. Martiarena, R.C. Salvarezza, Spontaneously formed sulfur adlayers on gold in electrolyte solutions: adsorbed sulfur or gold sulfide?, J. Phys. Chem. C 112 (2008) 11394–11402.
[12] E. Tosi, G.D. Ruano, S. Bengió, L. Salazar Alarcón, E.A. Sánchez, M. Khalid, O. Grizzi, M.L. Martiarena, G. Zampieri, Adsorption of S on the (111) surfaces of the noble metals Ag and Au studied by direct recoiling spectroscopy, Nucl. Instrum. Methods Phys. Res. Sect. B Beam Interact. with Mater. Atoms. 315 (2013) 55–59. http://dx.doi.org/10.1016/j.nimb.2013.04.084.
[13] G.M. Mcguirk, H. Shin, M. Caragiu, S. Ash, P.K. Bandyopadhyay, R.H. Prince, R.D. Diehl, Au(111) surface structures induced by adsorption: leed I(E) analysis of (1×1) and (5×5) Au(111)–S phases, Surf. Sci. 610 (2013) 42–47. http://dx.doi.org/10.1016/j.susc.2013.01.004.
[14] P.N. Abufager, G. Zampieri, K. Reuter, M.L. Martiarena, H.F. Busnengo, Long-range periodicity of S/Au(111) Structures At Low And Intermediate Coverages, J. Phys. Chem. C. 118 (2014) 290.
[15] R. Heinz, J.P. Rabe, Scanning tunneling microscopy investigation of sulfide and alkanethiolate adlayeres on Ag(111), Langmuir 11 (1995) 506–511.
[16] M. Yu, D.P. Woodruff, C.J. Satterley, R.G. Jones, V.R. Dhanak, Structural investigation of the interaction of molecular sulfur with Ag(111), J. Phys. Chem. C 111 (2007) 3152–3162.
[17] M. Shen, D. Liu, C.J. Jenks, P.A. Thiel, Novel self-organized structure of a Ag-S complex on the Ag(111) surface below room temperature, J. Phys. Chem. C 112 (2008) 4281–4290.
[18] M. Shen, D.-J. Liu, C.J. Jenks, P.A. Thiel, J.W. Evans, Accelerated coarsening of Ag adatom islands on Ag(111) due to trace amounts of S: mass-transport mediated by Ag-S complexes, J. Chem. Phys. 130 (2009) 094701. http://dx.doi.org/10.1063/1.3078033.
[19] S.M. Russell, D.-J. Liu, M. Kawai, Y. Kim, P.A. Thiel, Low-temperature adsorption of H_2S on Ag(111), J. Chem. Phys. 133 (2010) 124705. http://dx.doi.org/10.1063/1.3481481.
[20] A.J. Window, A. Hentz, D.C. Sheppard, G.S. Parkinson, D.P. Woodruff, T.C.Q. Noakes, P. Bailey, Silver sulphide growth on Ag(111): a medium energy ion scattering study, Surf. Sci. 604 (2010) 1254–1260. http://dx.doi.org/10.1016/j.susc.2010.04.009.
[21] L.A. Soria, G. Zampieri, M.L. Martiarena, Sulfur induced reconstruction of Ag(111) surfaces studied by DFT, J. Phys. Chem. C 115 (2011) 1–7.
[22] M. Shen, D. Liu, C.J. Jenks, P.A. Thiel, Comment on "sulfur-induced reconstruction of Ag(111) surfaces studied by DFT, J. Phys. Chem. C 115 (2011) (23651–23651).
[23] P.J. Feibelman, Formation and diffusion of S-decorated Cu clusters on Cu(111), Phys. Rev. Lett. 85 (2000) 606–609 ⟨http://www.ncbi.nlm.nih.gov/pubmed/10991351⟩.
[24] M.J. Harrison, D.P. Woodruff, J. Robinson, Density functional theory investigation of the structure of SO_2 and SO_3 on Cu(111) and Ni(111), Surf. Sci. 600 (2006) 1827–1836. http://dx.doi.org/10.1016/j.susc.2006.02.020.
[25] M.K. Bradley, D.P. Woodruff, J. Robinson, Surface Science Adsorbate-induced surface stress, surface strain and surface reconstruction: s on Cu(100) and Ni(100), Surf. Sci. 613 (2013) 21–27. http://dx.doi.org/10.1016/j.susc.2013.02.018.
[26] J. Jia, A. Bendounan, K. Chaouchi, V.A. Esaulov, Sulfur interaction with Cu(100) and Cu(111) surfaces: a photoemission study, J. Phys. Chem. C 118 (2014) 24583–24590. http://dx.doi.org/10.1021/jp5078517.
[27] T.E. Lister, J.L. Stickney, Atomic level studies of selenium electrodeposition on gold (111) and gold (110), J. Phys. Chem. 100 (1996) 19568–19576.
[28] S. Nagashima, Growth modes of Se overlayers deposited on Au(111) surfaces, Appl. Surf. Sci. 122 (1997) 116–119.
[29] B.M. Huang, T.E. Lister, J.L. Stickney, Se adlattices formed on Au(100), studies by LEED, AES, STM and electrochemistry, Surf. Sci. 392 (1997) 27–43. http://dx.doi.org/10.1016/S0039-6028(97)00413-5.
[30] J. Jia, A. Bendounan, H.M.N. Kotresh, K. Chaouchi, F. Sirotti, S. Sampath, V.A. Esaulov, Selenium Adsorption on Au(111) and Ag(111) surfaces: adsorbed Selenium and Selenide Films, J. Phys. Chem. C. 117 (2013) 9835–9842. http://dx.doi.org/10.1021/jp4007203.
[31] D.W. Suggs, J.L. Stickney, Characterization of atomic layers of tellurium electro-deposited on the low-index planes of gold, J. Phys. Chem. 95 (1991) 10056–10064.
[32] T. Jiang, Y. Tong, A. Bendounan, F. Nicolas, S. Kubsky, V.A. Esaulov, Selenium and benzeneselenol interaction with Cu(111), RSC Adv. 6 (2016) 84627–84633. http://dx.doi.org/10.1039/C6RA17334A.
[33] F.P. Cometto, C. Calderón, M. Morán, G. Ruano, H. Ascolani, G. Zampieri, P. Paredes-Olivera, E.M. Patrito, Formation, characterization, and stability of methaneselenolate monolayers on Au(111): an electrochemical high-resolution photoemission spectroscopy and DFT study, Langmuir. 30 (2014) 3754–3763. http://dx.doi.org/10.1021/la404996q.
[34] A linear background with a step after each peak. The two satellites of the Al Kα line were also considered in the fittings.
[35] J.J. Yeh, I. Lindau, Atomic subshell photoionization cross sections and asymmetry parameters: 1 < Z < 103, At. Data Nucl. Data Tables. 32 (1985).
[36] The atenuation length of the $Au5p_{3/2}$ photoelectrons is λ =18 Å [37]; therefore, the mean number of (111) planes contributing to the $Au5p_{3/2}$ signal is 7.7.
[37] P.H. Citrin, G. Wertheim, Y. Baer, Core-level binding energy and density of states from the surface atoms of gold, Phys. Rev. Lett. 41 (1978) 1425–1428. http://dx.doi.org/10.1103/PhysRevLett.41.1425.
[38] The Au4f7/2 peak was represented by a Doniach-Sunjic function with Lorentzian width 0.357 eV and asymmetry 0.052 [37]; the Gaussian width, left free during the fittings, was around1.1 eV in all the spectra.
[39] P. Zeppenfeld, K. Kern, R. David, G. Comsa, Diffraction from domain-wall systems, Phys. Rev. B. 38 (1988) 3918–3925.
[40] M.A. Van Hove, R.J. Koestner, P.C. Stair, J.P. Biberian, L.L. Kesmodel, I. Bartos,

G.A. Somorjai, The surface reconstruction of the (100) crystal faces of Iridium, platinum and gold, Surf. Sci. 103 (1981) 189–217.
[41] J.V. Barth, H. Brune, G. Ertl, R.J. Behm, STM observations of the reconstructed Au(111) surface: atomic structure, long-range superstructure, rotational domains, and surface defects, Phys. Rev. B 42 (1990) 9307–9318.
[42] Note that the substrate atoms do not enter into the LEED calculation and so only the relative positions of the adsorbates are significant. This means that the same result is obtained if the first Se atom (at the lower left corner of the cell) is placed on a hcp site; in this case, however, the Se atoms at the center of the cell would occupy "atop" sites, what is probably much higher in energy.
[43] The DFT calculations were performed within the generalized gradient approximation [44] using the Vienna Ab-initio Simulation Package (VASP) [45]. The Au(111) surface was modeled by a five-layer slab and 15 Å of vacuum space; the S and Se atoms were adsorbed only on one side of the slab. The positions of the adsorbates and of the Au atoms in the three top-most layers were allowed to relax until reaching forces smaller than 0.02 eV/ Å. The charge around the atoms (including core electrons) was calculated with the Bader method [46].
[44] J.P. Perdew, Y. Wang, Accurate and simple analytic representation of the electron-gas correlation energy, Phys. Rev. B. 45 (1992) 13244–13249. http://dx.doi.org/10.1103/PhysRevB.45.13244.
[45] (a) G. Kresse, J. Furthmüller, Efficient iterative schemes for ab initio total-energy calculations using a plane-wave basis set, Phys. Rev. B. 54 (1996) 11169–11186. http://dx.doi.org/10.1103/PhysRevB.54.11169;

(b) G. Kresse, D. Joubert, From ultrasoft pseudopotentials to the projector augmented-wave method, Phys. Rev. B. 59 (1999) 1758–1775. http://dx.doi.org/10.1103/PhysRevB.59.1758.
[46] (a) G. Henkelman, A. Arnaldsson, H. Jónsson, A fast and robust algorithm for Bader decomposition of charge density, Comput. Mater. Sci. 36 (2006) 0354–0360. http://dx.doi.org/10.1016/j.commatsci.2005.04.010;

(b) E. Sanville, S.D. Kenny, R. Smith, G. Henkelman, Improved grid-based algorithm for bader charge allocation, J. Comput. Chem. 28 (2007) 899. http://dx.doi.org/10.1002/jcc.
[47] S.B. Darling, A.W. Rosenbaum, Y. Wang, S.J. Sibener, Coexistence of the (23×√3) Au(111) Reconstruction and a striped phase self-assembled monolayer, Langmuir 18 (2002) 7462–7468.
[48] C. Bach, M. Giesen, H. Ibach, T. Einstein, Stress relief in reconstruction, Phys. Rev. Lett. 78 (1997) 4225–4228. http://dx.doi.org/10.1103/PhysRevLett.78.4225.
[49] M. Kostelitz, J.L. Domange, J. Oudar, Étude par la diffraction des électrons lents et la spectroscopie auger de l'adsorption du soufre sur L'Or, Surf. Sci. 36 (1973) 431–449. http://dx.doi.org/10.1016/0039-6028(73)90257-4.